

Universal Fermi velocity in highly compressed hydride superconductors

Evgueni F. Talantsev^{1,2*}

¹M.N. Mikheev Institute of Metal Physics, Ural Branch, Russian Academy of Sciences,
18, S. Kovalevskoy St., Ekaterinburg, 620108, Russia

²NANOTECH Centre, Ural Federal University, 19 Mira St., Ekaterinburg, 620002,
Russia

*corresponding author's E-mail: evgney.talantsev@imp.uran.ru

Abstract

Fermi velocity, v_F , is one of the primary characteristics of any conductor, including superconductors. For conductors at ambient pressure several experimental techniques have been developed to measure v_F and, for instance, Zhou *et al* (*Nature* **423** 398 (2003)) reported that high- T_c cuprates exhibit universal nodal Fermi velocity of $v_{F,univ} = (1.9 \pm 0.5) \times 10^5 \frac{m}{s}$. However, there were no experimental techniques applied to measure v_F in highly compressed near-room-temperature superconductors (NRTS), due to experimental challenges. Here to answer a question about the existence of the universal Fermi velocity in NRTS materials, we analyzed full inventory of the ground-state upper critical field data, $B_{c2}(0)$, for these materials and found that this class of superconductors exhibits universal Fermi velocity of $v_{F,univ} = \frac{1}{1.3} \times \left(\frac{2\Delta(0)}{k_B T_c} \right) \times 10^5 \frac{m}{s}$ (where $\Delta(0)$ is ground state amplitude of the energy gap). Due to the ratio of $\frac{2\Delta(0)}{k_B T_c}$ is varying within a narrow arrange of $3.2 \leq \frac{2\Delta(0)}{k_B T_c} \leq 5$, then $v_{F,univ}$ in NRTS materials is within the same ballpark with its high- T_c cuprates counterpart.

Universal Fermi velocity in highly compressed hydride superconductors

I. Introduction

Since pivotal experimental discovery of first near-room-temperature superconductor (NRTS) H₃S by Drozdov *et al* [1], nearly two dozen of highly compressed hydrogen-rich superconducting phases have been synthesized in binary and ternary systems [2-17]. Experimental studies of NRTS are well supported by first-principles calculations [18-30], however, experimental characterizations of NRTS phases are limited by narrow set of techniques, which can be applied for materials inside of diamond anvil cell (DAC) [25-27]. These techniques are X-ray diffraction (XRD) phase analysis, Raman spectroscopy and magnetoresistance measurements [31-35]. In some advanced experiments, Hall effect measurements can be also performed [31]. Based on this, only two characteristic values of the superconducting state of the NRTS phases are commonly extracted from the experimental data, which are the transition temperature, T_c , and the extrapolated value for the ground state upper critical field, $B_{c2}(0)$ or the ground state superconducting coherence length, $\xi(0)$, which can be derived from the Ginzburg-Landau [36] expression:

$$\xi(0) = \sqrt{\frac{\phi_0}{2\pi B_{c2}(0)}} \quad (1)$$

where $\phi_0 = \frac{h}{2e}$ is the superconducting flux quantum, h is Planck constant and e is electron electric charge.

Other important parameters of the NRTS materials, from which we can mention the Fermi velocity, v_F , cannot be measured to date, due to challenging experimental problems associated with measurement of this value for samples inside of DAC. However, considering that all NRTS superconductors are hydrides, there is an expectation, that these materials can exhibit universal Fermi velocity, $v_{F,univ}$, as the one was discovered in cuprates, $v_{F,univ} = (1.9 \pm 0.5) \times 10^5 \frac{m}{s}$ (which was reported by Zhou *et al* [37]). Partial theoretical background

for the quest for universal Fermi velocity in NRTS is based from one hand on recent understanding [38] that sulphur in H₃S is an analogue to the oxygen in cuprates, and from other hand that highly compressed hydrides are nicely added in main global scaling laws for superconductors [39-42].

Here, we reported the result of our search for universal Fermi velocity in NRTS materials which was based on the analysis of full inventory of the ground state upper critical field, $B_{c2}(0)$ in these materials. In the result, we found that universal Fermi velocity, $v_{F,univ}$, does exist in NRTS materials, and the one obeys the empirical law:

$$v_{F,univ} = \frac{1}{1.3} \times \frac{2\Delta(0)}{k_B T_c} \times 10^5 \left(\frac{m}{s} \right) \quad (2)$$

where k_B is the Boltzmann constant, and $\Delta(0)$ is the ground state superconducting energy gap.

II. Approach description

In Bardeen-Cooper-Schrieffer (BCS) theory of superconductivity [43] the ground state coherence length, $\xi(0)$, and the amplitude of the ground state energy gap, $\Delta(0)$, are linked through the expression:

$$\xi(0) = \frac{\hbar v_F}{\pi \Delta(0)} \quad (3)$$

where \hbar is reduced Planck constant. BCS theory also has a dimensionless ratio:

$$\alpha = \frac{2\Delta(0)}{k_B T_c} \quad (4)$$

By substituting Eqs. 3,4 in Eq. 1, one can get a dependence of the ground state upper critical field vs the transition temperature:

$$B_{c2}(0) = \left[\frac{\pi \phi_0 k_B^2}{8 \hbar^2} \right] \times \frac{\alpha^2}{v_F^2} \times T_c^2 \quad (5)$$

where the multiplicative pre-factor in square brackets is a constant:

$$A = \left[\frac{\pi \phi_0 k_B^2}{8 \hbar^2} \right] = 1.38 \times 10^7 \frac{T \times m^2}{s^2 \times K^2} \quad (6)$$

Thus, if hydrogen-rich superconductors exhibit universal Fermi velocity, $v_{F,univ}$, the fit of full inventory of $B_{c2}(0)$ vs T_c dataset to the equation of:

$$B_{c2}(0) = A \times f \times T_c^\beta \quad (7)$$

where β and $f = \frac{\alpha^2}{v_F^2}$ are free fitting parameters, should reveal that:

$$\beta \cong 2 \quad (8)$$

and if this is a case, then universal Fermi velocity, $v_{F,univ}$, can be calculated from deduced free-fitting parameter f :

$$v_{F,univ} = \frac{\alpha}{\sqrt{f}} = \frac{1}{\sqrt{f}} \times \frac{2\Delta(0)}{k_B T_c} \quad (9)$$

It should be noted, that $\alpha = \frac{2\Delta(0)}{k_B T_c}$ in highly-compressed hydrogen-rich superconductors is varying within a range [8,12,27,42,44-48]:

$$3.2 \leq \frac{2\Delta(0)}{k_B T_c} \leq 5 \quad (10)$$

(where the lower limit is the value deduced from experiment [42,44,48], while the upper limit is based on many results reported by the first-principles calculations, which always predict $4.3 \leq \frac{2\Delta(0)}{k_B T_c}$ [8,12,27,45-47] in NRTS materials).

III. Extrapolation model for the ground state upper critical field

Eq. 7 has the ground state upper critical field, $B_{c2}(0)$, as dependent variable. However, it is important to note that this value can be determined by the use of extrapolative models [49-53] which use experimental $B_{c2}(T)$ data measured at high reduced temperatures, $\frac{T}{T_c}$. Primary reason, why there is a necessity for extrapolative models, is that all highly-compressed hydrogen-rich superconductors have $B_{c2}(T \rightarrow 0 K) > 20 T$, which cannot be measured by conventional PPMS systems (manufactured by Quantum Design) where the highest magnetic

field is limited by $B_{\text{appl}} = 9\text{-}16$ Tesla (depends on the model). It should be also stressed, that $B_{c2}(T \rightarrow 0 \text{ K})$ for NRTS compounds of H_3S , LaH_{10} , YH_6/YH_9 and $(\text{La},\text{Y})\text{H}_{10}$ are so high, that even experimental data measured at world-top quasi-DC magnetic field facility [31,54] only covers the range of reduced temperatures $\frac{1}{2} \leq \frac{T}{T_c}$

From several available extrapolative $B_{c2}(T)$ models [49-53] in this paper we used analytical approximative expression for Werthamer-Helfand-Hohenberg (WHH) theory [55,56], which was proposed by Baumgartner *et al* [53] (and, thus, Eq. 11 we will designate as B-WHH model):

$$B_{c2}(T) = \frac{1}{0.693} \times \frac{\phi_0}{2\pi\xi^2(0)} \times \left(\left(1 - \frac{T}{T_c}\right) - 0.153 \times \left(1 - \frac{T}{T_c}\right)^2 - 0.152 \times \left(1 - \frac{T}{T_c}\right)^4 \right) \quad (11)$$

where $\xi(0)$ and $T_c \equiv T_c(B=0)$ are two free fitting parameters. Eq. 11 [53] was initially proposed to extrapolate $B_{c2}(T)$ data for neutron-irradiated Nb_3Sn alloys, and recently several research groups found that Eq. 11 is a good approximated tool for a variety of superconducting materials [4,57-62]. Based on this, in current study we used Eq. 11 as a good, robust and simple analytical tool to extrapolate $B_{c2}(T)$ curve on low temperature/high field region [4,57-62], because, as we mentioned above, $B_{c2}(T)$ datasets for NRTS superconductors are measured only at high reduced temperatures, $\frac{1}{2} \leq \frac{T}{T_c}$, because of experimental limitations.

There is a need to describe the criterion to extracting $B_{c2}(T)$ datasets from experimentally measured $R(T, B_{\text{appl}})$ curves. There are several criteria for the T_c , $B_{c2}(T)$ and $T_c(B_{\text{appl}})$ definition, which for the case of NRTS discussed recently in Ref. 63. In the result we found [63,64] that the best match between the electron-phonon coupling constant $\lambda_{\text{e-ph}}$ extracted from $R(T, B_{\text{appl}}=0)$ curves and $\lambda_{\text{e-ph}}$ computed by first principles calculation is when T_c is defining at as low as practically possible fraction of $R(T)/R_{\text{norm}}$ (where R_{norm} is the normal state resistance just above the transition). By analysing full inventory of $R(T, B_{\text{appl}})$ data for

NRTS materials herein, we came to conclusion that due to noise/slope issues of real-world $R(T, B_{\text{appl}})$ curves and a fact that highly-compressed superhydrides contained several superconducting phases the appropriate criterion, which we used in this study is:

$$\frac{R(T, B_{\text{appl}})}{R(T_c^{\text{onset}}, B_{\text{appl}})} = 0.05 \quad (12)$$

IV. Results

4.1. Unannealed highly-compressed sulphur hydride

In the first paper on NRTS superconductors, Drozdov *et al* [1] reported $R(T, B_{\text{appl}})$ data for unannealed highly-compressed sulphur hydride ($P = 155$ GPa) in their Figure 3(a). By using the criterion of Eq. 12 (which is $R(T, B_{\text{appl}})_{\text{criterion}} = 23 \text{ m}\Omega$ for given $R(T, B_{\text{appl}})$ curves showed in bottom insert in Figure 3(a) in Ref. 1), we extracted $B_{c2}(T)$ dataset for this sample, which is shown in Fig. 1. Because this $B_{c2}(T)$ dataset covers significant part of full temperature range, $0 \text{ K} < T \leq T_c$, there was no need to use extrapolative fit and instead we fitted this dataset to the model [48], which allows to deduce $\Delta(0)$, $\frac{2\Delta(0)}{k_B T_c}$, $\Delta C/C$ (which is the relative jump in electronic specific heat at T_c):

$$B_{c2}(T) = \frac{\phi_0}{2\pi\xi^2(0)} \times \left(\frac{1.77 - 0.43\left(\frac{T}{T_c}\right)^2 + 0.07\left(\frac{T}{T_c}\right)^4}{1.77} \right)^2 \times \left[1 - \frac{1}{2k_B T} \times \int_0^\infty \frac{d\varepsilon}{\cosh^2\left(\frac{\sqrt{\varepsilon^2 + \Delta^2(T)}}{2k_B T}\right)} \right] \quad (13)$$

where temperature dependent superconducting gap, $\Delta(T)$, is given by [65,66]:

$$\Delta(T) = \Delta(0) \times \tanh \left[\frac{\pi k_B T_c}{\Delta(0)} \times \sqrt{\eta \times \frac{\Delta C}{C} \times \left(\frac{T_c}{T} - 1 \right)} \right] \quad (14)$$

where $\eta = 2/3$ for s -wave superconductors.

Eqs. 13,14 were used to extract $\xi(0)$, $\Delta(0)$, T_c and $\frac{\Delta C}{C}$ from $B_{c2}(T)$ datasets in a variety of superconductors, for instance, for two highly-compressed hydrides phases of H_3S [48] and of SnH_{12} [42], V_3Si [67], and several iron-based superconductors [67]. However, it should be

stressed that the approach (i.e. Eq. 13,14) is only applicable for $B_{c2}(T)$ datasets defined by Eq. 12 or by stricter criterion.

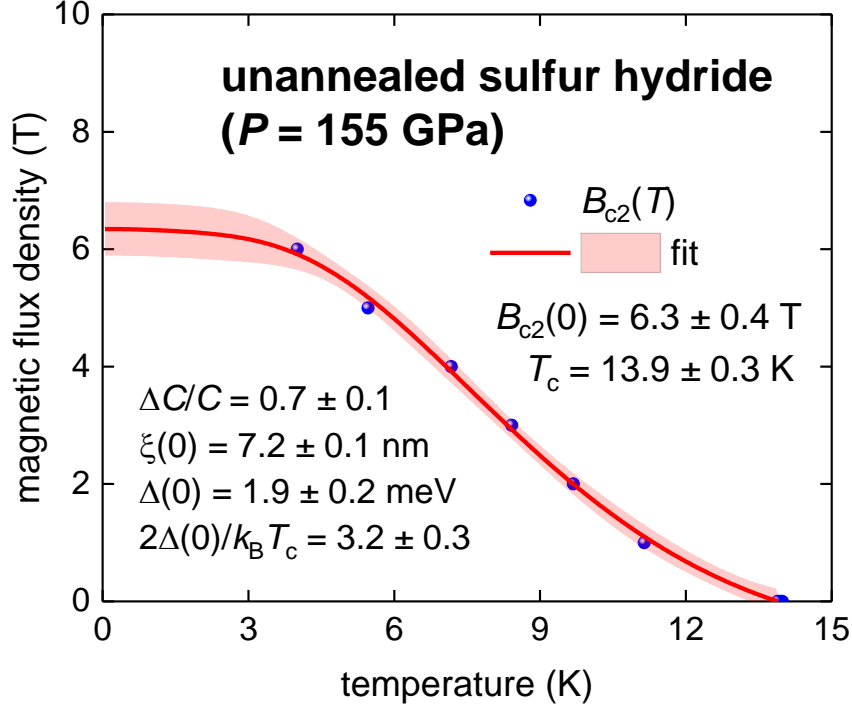


Figure 1. The upper critical field data, $B_{c2}(T)$, and data fit to Eqs. 13,14 for unannealed highly-compressed sulphur hydride ($P = 190$ GPa). Raw $R(T, B_{\text{appl}})$ dataset reported by Drozdov *et al* [1]. Deduced values are shown in the figure. 95% confidence bands are shown by a pink shaded area. Fit quality is $R = 0.9985$.

One of the most important deduced parameters, $\alpha = \frac{2\Delta(0)}{k_B T_c} = 3.2 \pm 0.3$, is in remarkable agreement with counterpart values deduced for highly-compressed annealed H_3S ($P = 155$ - 160 GPa), $\frac{2\Delta(0)}{k_B T_c} = 3.20 \pm 0.02$ [44] and $\frac{2\Delta(0)}{k_B T_c} = 3.55 \pm 0.31$ [48], and for highly-compressed annealed SnH_{12} ($P = 190$ GPa), $\frac{2\Delta(0)}{k_B T_c} = 3.28 \pm 0.18$ [42]. Deduced $\frac{\Delta C}{C} = 0.7 \pm 0.1$ is also below the weak-coupling limit of BCS theory $\frac{\Delta C}{C} = 1.43$, as its counterpart in the annealed H_3S material, $\frac{\Delta C}{C} = 1.2 \pm 0.3$ [48]. It should be mentioned that to deduce $\frac{\Delta C}{C}$ with higher accuracy requires more $B_{c2}(T)$ datapoints, especially at $T \sim T_c$. Deduced $B_{c2}(0)$ and T_c are included in Table I.

4.2. Annealed highly-compressed sulphur hydride

Mozaffari *et al* [31] reported extended $R(T, B_{\text{appl}})$ datasets for annealed highly-compressed sulphur hydride ($P = 155, 160$ GPa). By using the criterion of Eq. 12, we extracted $B_{c2}(T)$ datasets which are shown in Figure 2, together with the fits to B-WHH model (Eq. 11). Deduced $B_{c2}(0)$ and T_c values are included in Table I.

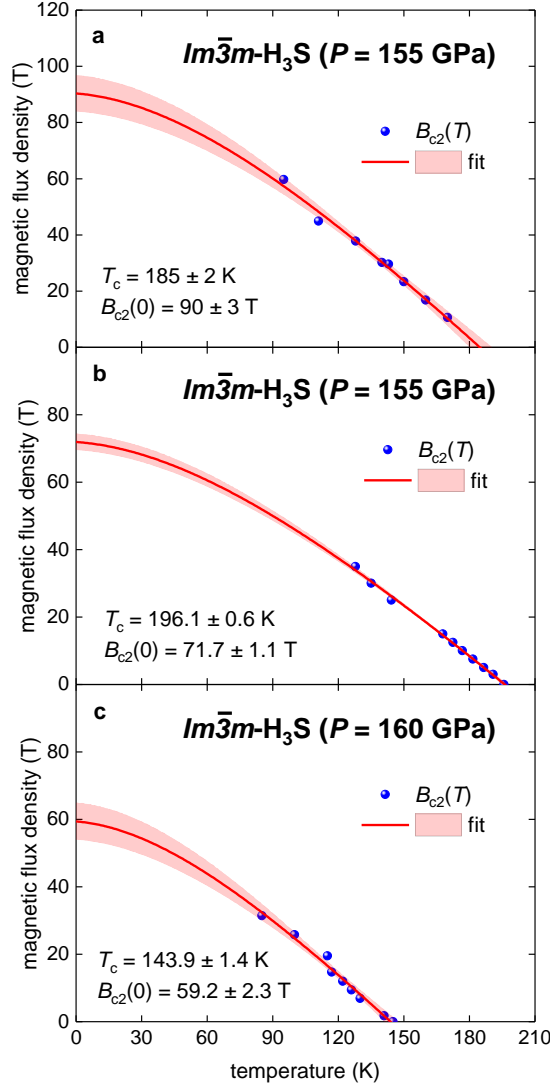


Figure 2. The upper critical field, $B_{c2}(T)$, data for highly-compressed $Im\bar{3}m$ -H₃S phase at $P = 155$ GPa (a,b) and $P = 160$ GPa (c) and data fit to B-WHH model [53] (Eq. 11). Raw $R(T, B_{\text{appl}})$ datasets reported by Mozaffari *et al* [31]. Fits quality are (a) $R = 0.9892$; (b) $R = 0.9974$; (c) $R = 0.9837$. 95% confidence bands are shown by pink shaded areas.

4.3. Annealed highly-compressed cerium hydrides

Chen *et al* [12] reported on the observation high-temperature superconductivity in superhydrides of cerium. By using the criterion of Eq. 12, we extracted $B_{c2}(T)$ datasets from

four $R(T, B_{\text{appl}})$ curves reported by Chen *et al* [12] and fitted these $B_{c2}(T)$ datasets to B-WHH model (Eq. 11) in Figure 3. Deduced $B_{c2}(0)$ and T_c values are included in Table I.

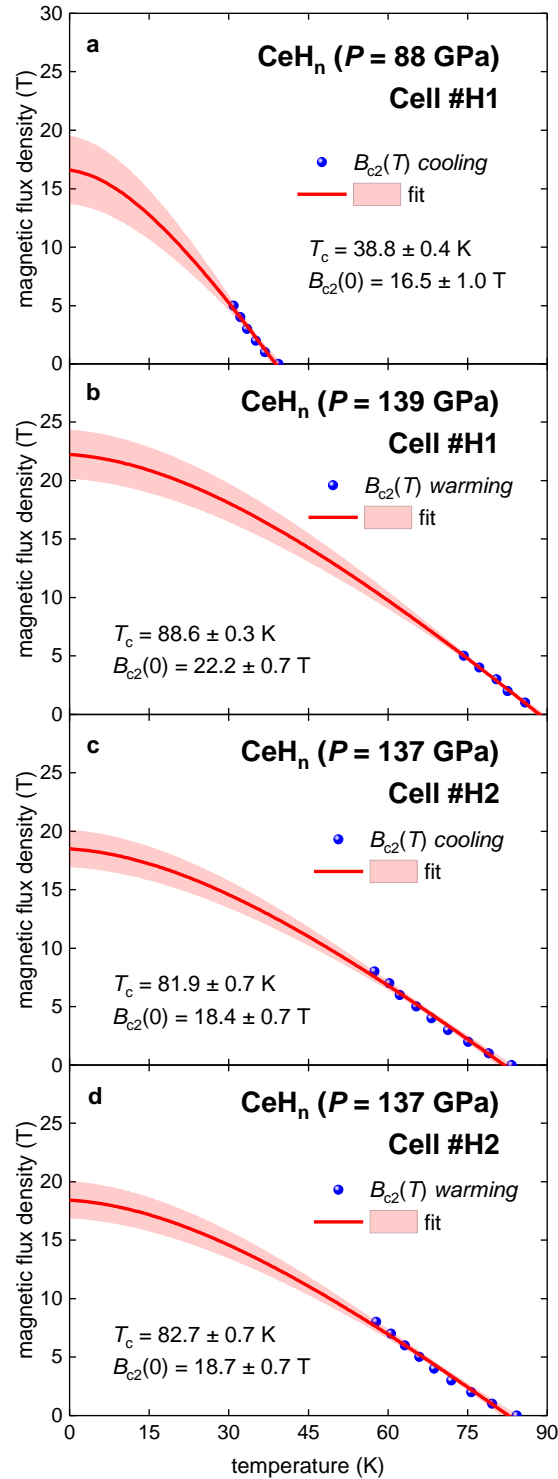


Figure 3. The upper critical field, $B_{c2}(T)$, data for highly-compressed superhydrides of cerium and data fits to Eq. 11. Raw $R(T, B_{\text{appl}})$ datasets reported by Chen *et al* [12]. (a) Raw $R(T, B_{\text{appl}})$ data reported in Fig. S7(a) [12], fit quality is $R = 0.9792$. (b) Raw $R(T, B_{\text{appl}})$ data reported in Fig. 1(c) [12], fit quality is $R = 0.9966$. (c,d) Raw $R(T, B_{\text{appl}})$ data reported in Fig. 1(d) [12], fit quality is $R = 0.9860$ (c) and $R = 0.9859$ (d). 95% confidence bands are shown by pink shaded areas.

4.4. Annealed highly-compressed LaH₁₀

Sun *et al* [54] reported results of magnetoresistance studies for two phases of highly-compressed LaH₁₀. By using the criterion of Eq. 12, we extracted $B_{c2}(T)$ datasets for these two phases and fitted these $B_{c2}(T)$ datasets to B-WHH model (Eq. 11) in Figure 4. Deduced $B_{c2}(0)$ and T_c values are included in Table I.

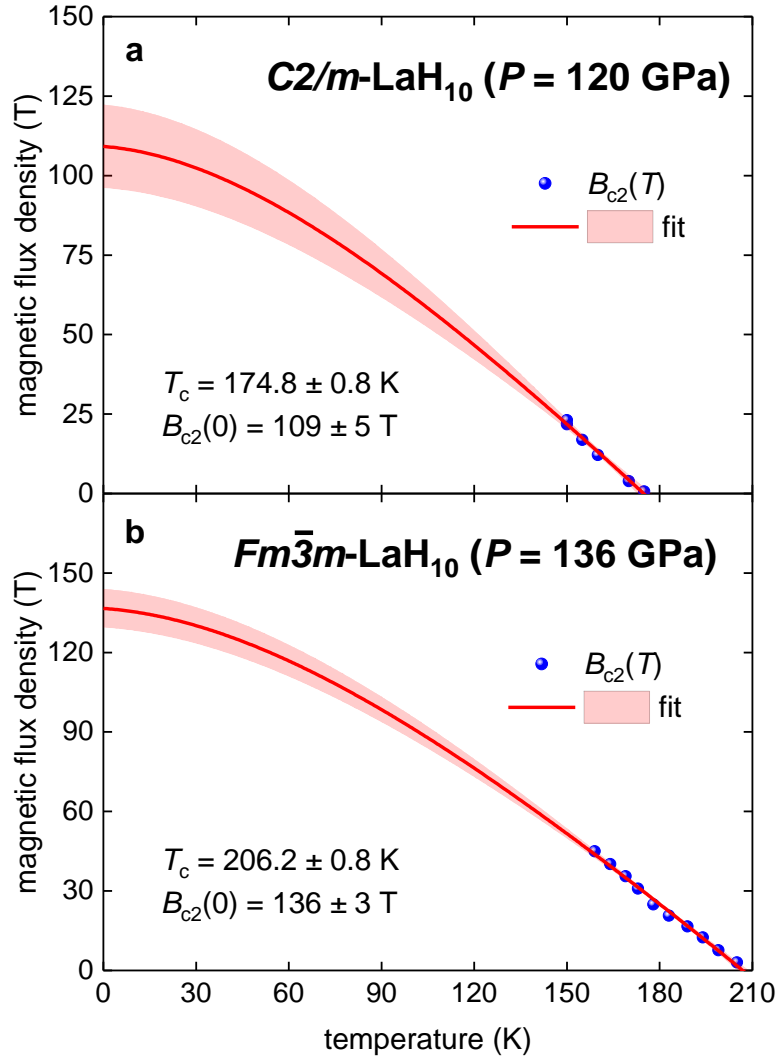


Figure 4. The upper critical field, $B_{c2}(T)$, data for highly-compressed LaH₁₀ and data fits to Eq. 11. Raw $R(T, B_{\text{appl}})$ datasets reported by Sun *et al* [49]. (a) Raw $R(T, B_{\text{appl}})$ data reported in Fig. 3(a) [54], fit quality is $R = 0.9907$. (b) Raw $R(T, B_{\text{appl}})$ data reported in Fig. 3(b) [54], fit quality is $R = 0.9941$. 95% confidence bands are shown by pink shaded areas.

4.5. Annealed highly-compressed YH₆/YD₆

Recently, Troyan *et al* [4] and Kong *et al* [5] reported on the discovery of new highly-compressed NRTS polyhydrides/polydeuterides of yttrium, YH_n/YD_n (n = 4,6,7,9). Here in Figure 5 we showed extracted $B_{c2}(T)$ for YD₆ ($P = 172$ GPa, raw $R(T, B_{\text{appl}})$ dataset is from Figure S13(a) [4]) and for YH₆ ($P = 200$ GPa, raw $R(T, B_{\text{appl}})$ dataset is from Figure S16(a) [4]) and data fits to B-WHH model (Eq. 11). Deduced $B_{c2}(0)$ and T_c are included in Table I.

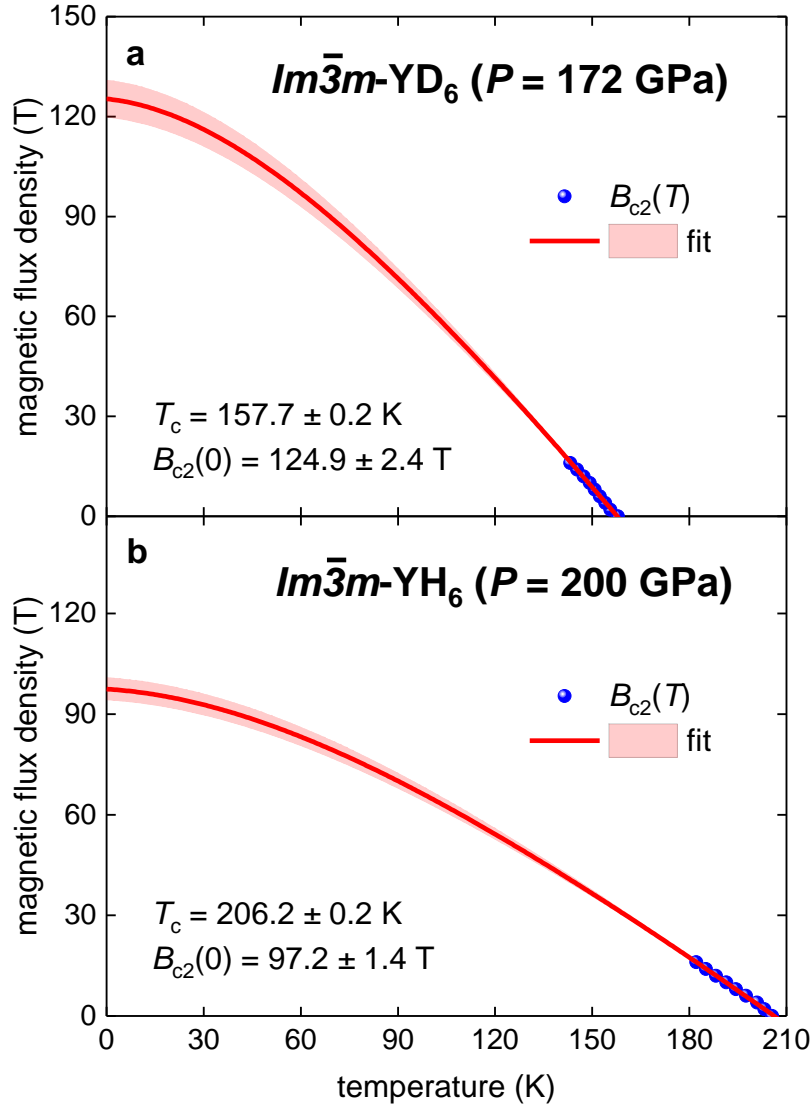


Figure 5. The upper critical field, $B_{c2}(T)$, data for highly-compressed YH₆/YD₆ and fits to Eq. 11. Raw $R(T, B_{\text{appl}})$ datasets reported by Troyan *et al* [4]. (a) Raw $R(T, B_{\text{appl}})$ data reported in Fig. S13(a) [4], fit quality is $R = 0.9971$. (b) Raw $R(T, B_{\text{appl}})$ data reported in Fig. S16(a) [4], fit quality is $R = 0.9982$. 95% confidence bands are shown by pink shaded areas.

4.6. Annealed highly-compressed ternary (La,Y)H₁₀

Semenok *et al* [8] reported on the discovery of new ternary NRTS polyhydride of (Y,Lu)H₁₀. In Figure 6 we showed extracted $B_{c2}(T)$ datasets for (Y,Lu)H₁₀ phase and data fits to B-WHH model (Eq. 11). Deduced $B_{c2}(0)$ and T_c for this phase are included in Table I.

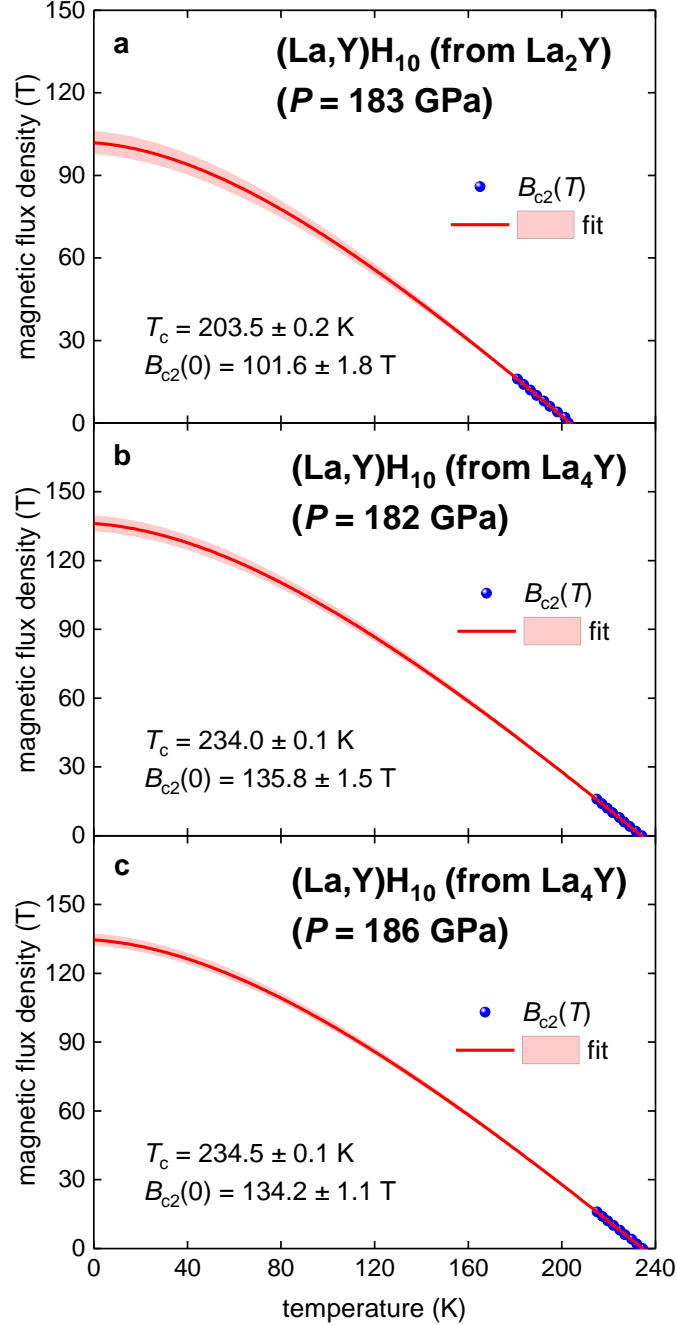


Figure 6. The upper critical field, $B_{c2}(T)$, data for highly-compressed (La,Y)H₁₀ and fits to Eq. 11. Raw $R(T, B_{\text{appl}})$ datasets reported by Semenok *et al* [8]. (a) Raw $R(T, B_{\text{appl}})$ data reported in Fig. S27(b) [8], fit quality is $R = 0.9975$. (b) Raw $R(T, B_{\text{appl}})$ data reported in Fig. S28(a) [8], fit quality is $R = 0.9991$. (c) Raw $R(T, B_{\text{appl}})$ data reported in Fig. S28(a) [8], fit quality is $R = 0.9995$. 95% confidence bands are shown by pink shaded areas.

4.7. Annealed highly-compressed SnH₁₂

Recently, Hong *et al* [11] reported on the discovery of a new superconducting polyhydride of C2/*m*-SnH₁₂ ($P = 190$ GPa). Extracted $B_{c2}(T)$ datasets for this phase we already reported in our previous work (Table I in Ref. 41). Here in Figure 7 we fitted these datasets to B-WHH model (Eq. 11). Deduced $B_{c2}(0)$ and T_c for this phase are included in Table I.

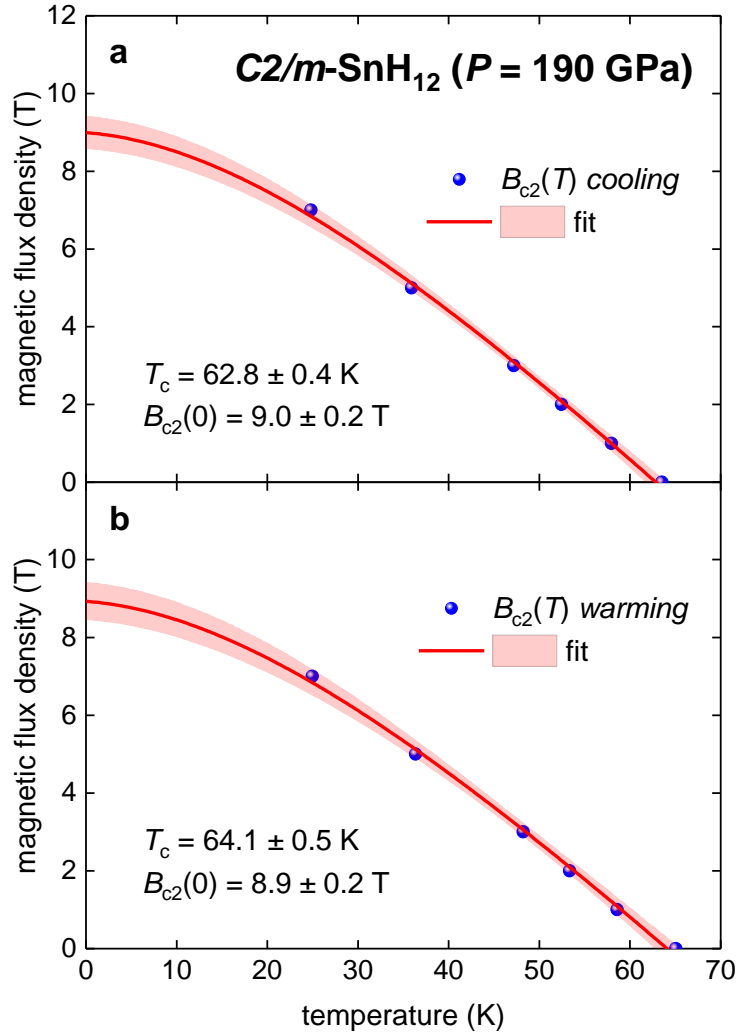


Figure 7. The upper critical field data, $B_{c2}(T)$, and data fit to Eq. 11 for C2/*m*-SnH₁₂ ($P = 190$ GPa). Raw $R(T, B_{\text{appl}})$ datasets reported by Hong *et al* [11] and extracted $B_{c2}(T)$ datasets can be found in Table I in Ref. 41. (a) fit quality is $R = 0.9971$; (b) fit quality is $R = 0.9978$.

4.8. Annealed highly-compressed ThH₉ and ThH₁₀

Semenok *et al* [16] reported on the discovery of a new NRTS polyhydrides of thorium, ThH₉ and ThH₁₀. Raw $R(T, B_{\text{appl}})$ dataset for mixture of ThH₉ and ThH₁₀ phases is in Figure 5(c) in Ref. [16]. To deduce $B_{c2}(T)$ dataset for phase ThH₁₀ we used the criterion of $R(T, B_{\text{appl}})_{\text{criterion}} = 4.9 \text{ m}\Omega$, while to deduce $B_{c2}(T)$ dataset for phase ThH₉ we used the criterion of $R(T, B_{\text{appl}})_{\text{criterion}} = 0.46 \text{ m}\Omega$. In Figure 7 we fitted these datasets to B-WHH model (Eq. 11). Deduced $B_{c2}(0)$ and T_c for this phase are included in Table I.

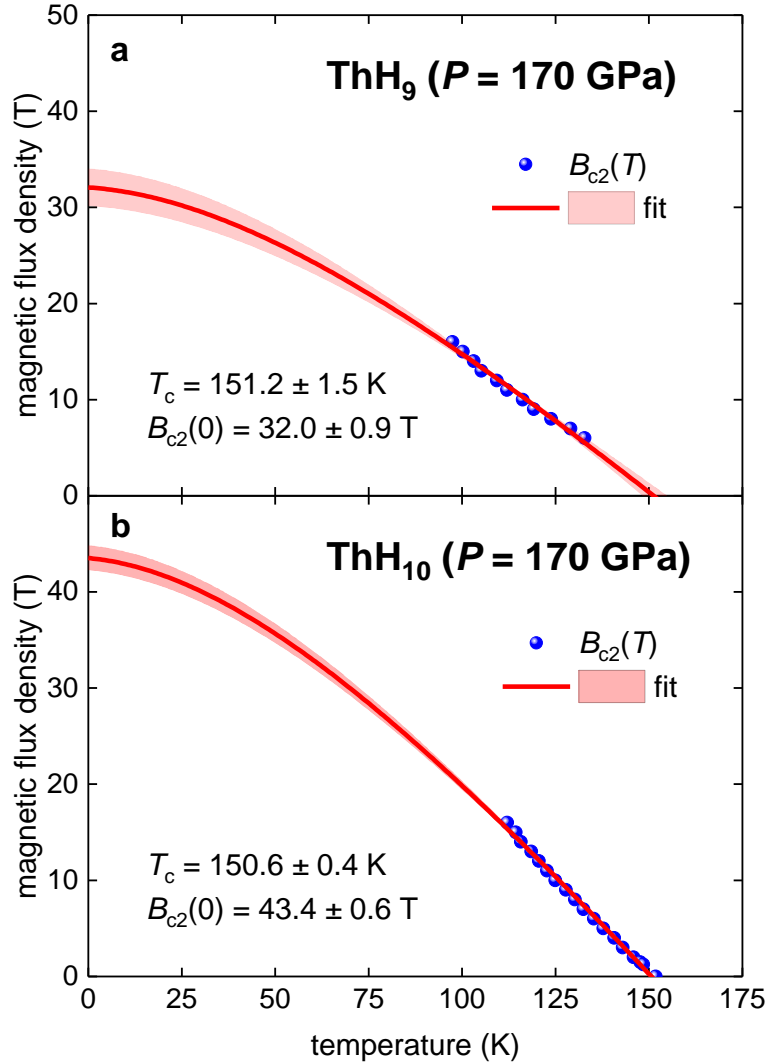


Figure 8. The upper critical field data, $B_{c2}(T)$, and data fit to Eq. 11 for NRTS phases of (a) ThH₉ and (b) ThH₁₀. Raw $R(T, B_{\text{appl}})$ datasets reported by Semenok *et al* [16] in their Figure 5(c). (a) fit quality is $R = 0.9866$; (b) fit quality is $R = 0.9957$.

4.9. Analysis of $B_{c2}(0)$ vs T_c for superhydride phases

All deduced $B_{c2}(0)$ and T_c values for superhydride phases are collected in Table I, where we also added data for Th_4H_{15} phase reported by Satterthwaite and Toepke [68].

Table I. Deduced $B_{c2}(0)$ and T_c values for hydrogen-rich superconductors for which raw $R(T, B_{\text{appl}})$ data are available to date (references are included).

Phase and Data Source	Figure No.	Pressure (GPa)	T_c (K)	ΔT_c (K)	$B_{c2}(0)$ (T)	$\Delta B_{c2}(0)$ (T)
Unannealed sulphur hydride (Fig. 3(a) in Ref. 1)	1	155	13.9	0.3	6.3	0.4
Annealed H_3S (Fig. 3 in Ref. 31)	2(a)	155	185	2	98.8	1.2
Annealed H_3S (Figs. S1,S2 in Ref. 31)	2(b)	155	196.1	0.6	71.1	1.1
Annealed H_3S (Fig. 3 in Ref. 31)	2(c)	160	143.9	1.4	59.2	2.3
Annealed CeH_9 (Fig. S7(a) in Ref. 12) cooling	3(a)	88	38.8	0.4	16.5	1
Annealed CeH_9 (Fig. 1(c) in Ref. 12) warming	3(b)	139	88.6	0.3	22.2	0.7
Annealed CeH_9 (Fig. 1(d) in Ref. 12) cooling	3(c)	137	81.9	0.7	18.4	0.7
Annealed CeH_9 (Fig. 1(d) in Ref. 12) warming	3(d)	137	82.7	0.7	18.7	0.6
Annealed LaH_{10} (Fig. 3(a) in Ref. 47)	4(a)	120	174.8	0.8	90	3
Annealed LaH_{10} (Fig. 3(b) in Ref. 47)	4(b)	136	206.2	0.8	136	3
Annealed YD_6 (Fig. S13(a) in Ref. 4)	5(a)	172	157.7	0.2	124.9	2.4
Annealed YH_6 (Fig. S16(c) in Ref. 4)	5(b)	200	206.2	0.2	97.2	1.4
Annealed $(\text{La}, \text{Y})\text{H}_{10}$ (Fig. S27(b) in Ref. 8)	6(a)	183	203.5	0.2	101.6	1.8
Annealed $(\text{La}, \text{Y})\text{H}_{10}$ (Fig. S28(a) in Ref. 8)	6(b)	182	234	0.1	135.8	1.5
Annealed $(\text{La}, \text{Y})\text{H}_{10}$ (Fig. S28(a) in Ref. 8)	6(c)	186	234.5	0.1	134	1
Annealed SnH_{12} (Fig. 4(a) in Ref. 11) cooling	7(a)	190	62.8	0.4	9	0.2
Annealed SnH_{12} (Fig. 4(a) in Ref. 11) warming	7(b)	190	64.1	0.5	8.9	0.2
Annealed ThH_9 (Fig. 4(a) in Ref. 16)	8(a)	170	151.2	1.5	32	0.9
Annealed ThH_{10} (Fig. 4(a) in Ref. 16)	8(b)	170	150.6	0.4	43.4	0.6
Th_4H_{15} (Ref. 68)		ambient	8.2	0.15	2.75	0.25

Full dataset from Table I is shown in Figure 9 together with the fit to Eq. 7. Despite a fact that this dataset has a large scattering, it can be seen in Figure 9(a), that free-fitting power-law exponent, $\beta = 2.07 \pm 0.14$, is practically undistinguishable from expected $\beta \equiv 2$ value (Eq. 5). For the case when β is free-fitting parameter (Figure 9(a)), deduced $f = (1.19 \pm 0.90) \times 10^{-10} \frac{\text{m}^2}{\text{s}^2}$ has a large uncertainty. However, when β is fixed to 2 (Figure 9(b)), free-fitting parameter f can be deduced with high accuracy:

$$f = \frac{\alpha^2}{v_{F,univ}^2} = (1.68 \pm 0.08) \times 10^{-10} \frac{s^2}{m^2} \quad (15)$$

From Equation 15, one can obtain:

$$v_{F,univ} = \frac{\alpha}{(1.30 \pm 0.03)} \times 10^5 \frac{m}{s} \cong \frac{1}{1.3} \times \frac{2\Delta(0)}{k_B T_c} \times 10^5 \frac{m}{s} \quad (16)$$

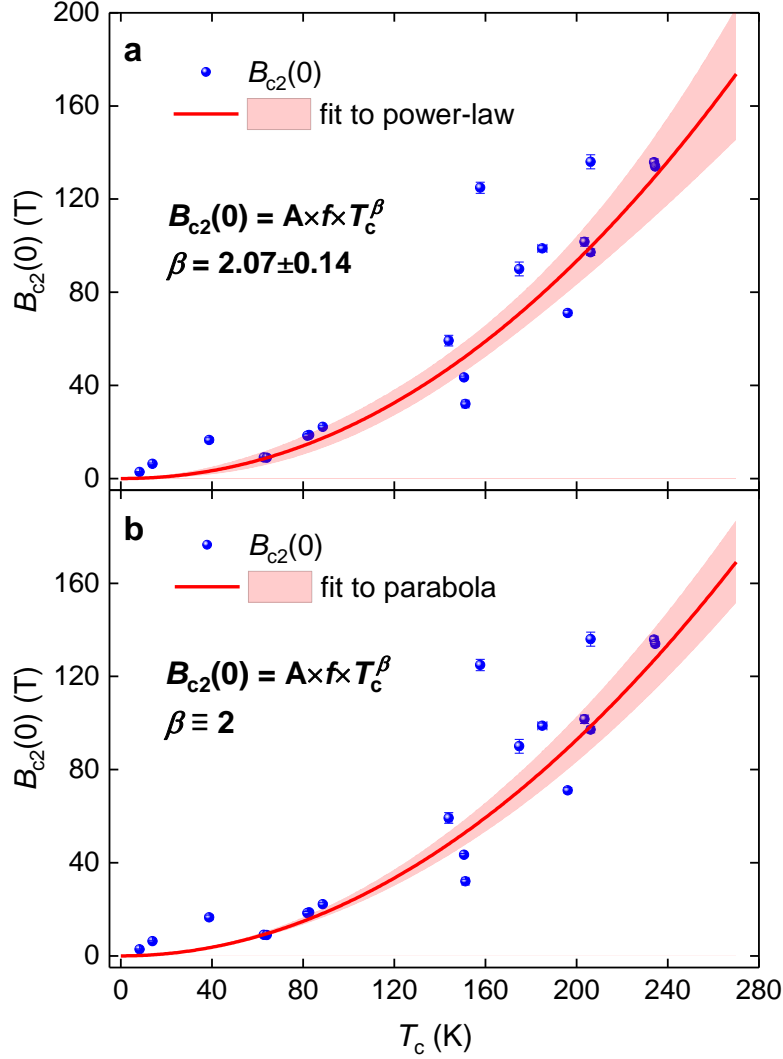


Figure 9. Total $B_{c2}(0)$ vs T_c dataset for hydrogen-rich superconductors deduced in this work (Table I) and data fit to (a) Eq. 7 and (b) Eq. 5. (a) – free-fitting $\beta = 2.07 \pm 0.14$ and $f = (1.19 \pm 0.90) \times 10^{-10} \frac{s^2}{m^2}$, fit quality is $R = 0.9361$. (b) – $\beta = 2.0$ (fixed) and free-fitting $(1.68 \pm 0.08) \times 10^{-10} \frac{s^2}{m^2}$, fit quality is $R = 0.9354$.

Deduced $v_{F,univ}$ for hydrogen-rich superconductors (Eq. 16) is at the same ballpark as its counterpart for high- T_c cuprates $v_{F,univ} = (1.9 \pm 0.5) \times 10^5 \frac{m}{s}$ [37], if one takes into account Eq. 10.

V. Conclusions

In this study we proposed that hydrogen-rich superconductors, including near-room-temperature superconductors, form distinguished subclass of superconducting materials, which exhibits universal Fermi velocity, v_F , which is given by empirical expression of:

$$v_{F,univ} = \frac{1}{1.3} \times \frac{2\Delta(0)}{k_B T_c} \times 10^5 \frac{m}{s}.$$

Acknowledgement

The author thanks financial support provided by the Ministry of Science and Higher Education of Russia (theme “Pressure” No. AAAA-A18-118020190104-3) and by Act 211 Government of the Russian Federation, contract No. 02.A03.21.0006.

Data Availability Statement

No new data were created or analysed in this study. Data sharing is not applicable to this article.

References

- [1] A. P. Drozdov, M.I. Erements, I.A. Troyan, V. Ksenofontov, S. I. Shylin, Conventional superconductivity at 203 kelvin at high pressures in the sulfur hydride system *Nature* **525**, 73-76 (2015)
- [2] A. P. Drozdov, *et al* Superconductivity at 250 K in lanthanum hydride under high pressures *Nature* **569**, 528-531 (2019)
- [3] M. Somayazulu, *et al* Evidence for superconductivity above 260 K in lanthanum superhydride at megabar pressures *Phys. Rev. Lett.* **122** 027001 (2019)
- [4] I. A. Troyan, *et al* Anomalous high-temperature superconductivity in YH₆ *Adv. Mater.* **33** 2006832 (2021)
- [5] P. P. Kong, *et al* Superconductivity up to 243 K in yttrium hydrides under high pressure *Nature Communications* **12**, 5075 (2021)
- [6] L. Ma, *et al* Experimental observation of superconductivity at 215 K in calcium superhydride under high pressure (arXiv:2103.16282)
- [7] Z. W. Li, *et al* Superconductivity above 200 K observed in superhydrides of calcium (arXiv:2103.16917)

- [8] D. V. Semenov, *et al* Superconductivity at 253 K in lanthanum–yttrium ternary hydrides *Materials Today* **48**, 18-28 (2021)
- [9] A. P. Drozdov, M. I. Erements and I. A. Troyan, Superconductivity above 100 K in PH_3 at high pressures (arXiv:1508.06224) [26] D. Zhou, *et al.* Superconducting praseodymium superhydrides *Sci. Adv.* **6**, eaax6849 (2020)
- [10] T. Matsuoka, *et al.* Superconductivity of platinum hydride *Phys. Rev. B* **99**, 144511 (2019)
- [11] F. Hong, *et al.* Superconductivity at ~ 70 K in tin hydride SnH_x under high pressure *Materials Today Physics* **22** 100596 (2022)
- [12] W. Chen, D. V. Semenov, X. Huang, H. Shu, X. Li, D. Duan, T. Cui and A. R. Oganov, High-temperature superconducting phases in cerium superhydride with a T_c up to 115 K below a pressure of 1 Megabar, *Phys. Rev. Lett.* **127**, 117001 (2021)
- [13] M. Sakata, *et al.* Superconductivity of lanthanum hydride synthesized using AlH_3 as a hydrogen source *Superconductor Science and Technology* **33** 114004 (2020)
- [14] W. Chen, *et al.* High-pressure synthesis of barium superhydrides: Pseudocubic BaH_{12} *Nature Communications* **12**, 273 (2021)
- [15] M. A. Kuzovnikov and M. Tkacz, High-pressure synthesis of novel polyhydrides of Zr and Hf with a Th_4H_{15} -type structure *J. Phys. Chem. C* **123**, 30059–30066 (2019)
- [16] D. V. Semenov, *et al.* Superconductivity at 161 K in thorium hydride ThH_{10} : synthesis and properties *Mater. Today* **33**, 36–44 (2020)
- [17] N. Wang, *et al.* A low- T_c superconducting modification of Th_4H_{15} synthesized under high pressure *Superconductor Science and Technology* **34** 034006 (2021)
- [18] H. Xie, *et al.* Superconducting zirconium polyhydrides at moderate pressures *J. Phys. Chem. Lett.* **11**, 646–651 (2020)
- [19] S. Mengyao, *et al.* Superconducting ScH_3 and LuH_3 at megabar pressures *Inorganic Chemistry* (2021); in press: <https://doi.org/10.1021/acs.inorgchem.1c01960>
- [20] J. Chen, *et al.* Computational design of novel hydrogen-rich YS–H compounds *ACS Omega* **4** 14317-14323 (2019)
- [21] J. A. Alarco, P. C. Talbot and I. D. R. Mackinnon, Identification of superconductivity mechanisms and prediction of new materials using Density Functional Theory (DFT) calculations *J. Phys.: Conf. Ser.* **1143**, 012028 (2018)
- [22] D. V. Semenov, A. G. Kvashnin, I. A. Kruglov, and A. R. Oganov, Actinium hydrides AcH_{10} , AcH_{12} , and AcH_{16} as high-temperature conventional superconductors *J. Phys. Chem. Lett.* **9** 1920-1926 (2018)
- [23] C. J. Pickard, I. Errea, and M. I. Erements, Superconducting hydrides under pressure *Annual Review of Condensed Matter Physics* **11**, 57-76 (2020).
- [24] J. A. Flores-Livas, L. Boeri, A. Sanna, G. Profeta, R. Arita, M. Erements. A perspective on conventional high-temperature superconductors at high pressure: Methods and materials. *Physics Reports* **856**, 1-78 (2020).
- [25] A. Goncharov, Phase diagram of hydrogen at extreme pressures and temperatures; updated through 2019 (Review article), *Low Temperature Physics* **46**, 97 (2020).
- [26] E. Gregoryanz, C. Ji, P. Dalladay-Simpson, B. Li, R. T. Howie, and H.-K. Mao, Everything you always wanted to know about metallic hydrogen but were afraid to ask. *Matter and Radiation at Extremes* **5**, 038101 (2020).
- [27] L. Boeri, *et al.* The 2021 room-temperature superconductivity roadmap. *Journal of Physics: Condensed Matter* (2021), accepted manuscript: <https://doi.org/10.1088/1361-648X/ac2864>
- [28] X. Zhang, Y. Zhao, G. Yang, Superconducting ternary hydrides under high pressure *WIREs Computational Molecular Science* (2021) in press: <https://doi.org/10.1002/wcms.1582>

- [29] M. Dogan and M. L. Cohen, Anomalous behaviour in high-pressure carbonaceous sulfur hydride *Physica C* 1353851 (<https://doi.org/10.1016/j.physc.2021.1353851>) (2021)
- [30] T. Wang, *et al.* Absence of conventional room temperature superconductivity at high pressure in carbon doped H₃S *arXiv:2104.03710* (2021)
- [31] S. Mozaffari, *et al* Superconducting phase diagram of H₃S under high magnetic fields *Nat. Commun.* **10** 2522 (2019)
- [32] V. S. Minkov, V. B. Prakapenka, E. Greenberg, M. I. Erements, Boosted T_c of 166 K in superconducting D₃S synthesized from elemental sulfur and hydrogen *Angew. Chem. Int. Ed.*, **59**, 18970-18974 (2020)
- [33] R. Matsumoto, *et al.* Electrical transport measurements for superconducting sulfur hydrides using boron-doped diamond electrodes on bevelled diamond anvil *Superconductor Science and Technology* **33** 124005 (2020)
- [34] D. Laniel, *et al.* Novel sulfur hydrides synthesized at extreme conditions *Phys. Rev. B* **102**, 134109 (2020)
- [35] X. Huang, *et al.* High-temperature superconductivity in sulfur hydride evidenced by alternating-current magnetic susceptibility *National Science Review* **6** 713-718 (2019)
- [36] V. L. Ginzburg and L.D. Landau, *Zh. Eksp. Teor. Fiz.* **20**, 1064 (1950).
- [37] X. J. Zhou, *et al*, High-temperature superconductors: Universal nodal Fermi velocity *Nature* **423** 398 (2003).
- [38] D. K. Sunko, High-temperature superconductors as ionic metals *Journal of Superconductivity and Novel Magnetism* **33**, 27-33 (2020)
- [39] D. R. Harshman and A. T. Fiory, High- T_c superconductivity in hydrogen clathrates mediated by Coulomb interactions between hydrogen and central-atom electrons *Journal of Superconductivity and Novel Magnetism* **33**, 2945-2961 (2020)
- [40] D. R. Harshman and A. T. Fiory, The superconducting transition temperatures of C-S-H based on inter-sublattice S–H₄-tetrahedron electronic interactions *Journal of Applied Physics* **131**, 015105 (2022)
- [41] Y. J. Uemura, Bose-Einstein to BCS crossover picture for high- T_c cuprates *Physica C* **282–287**, 194-197 (1997)
- [42] E. F. Talantsev, Comparison of highly-compressed C₂/m-SnH₁₂ superhydride with conventional superconductors *J. Phys.: Condens. Matter* **33** 285601 (2021)
- [43] J. Bardeen, L N Cooper, and J R Schrieffer, Theory of superconductivity *Phys. Rev.* **108**, 1175-1204 (1957)
- [44] E. F. Talantsev, W. P. Crump, J. G. Storey, J. L. Tallon, London penetration depth and thermal fluctuations in the sulphur hydride 203 K superconductor *Annalen der Physik* **529** 1600390 (2017)
- [45] I. Errea, *et al*, Quantum crystal structure in the 250-kelvin superconducting lanthanum hydride *Nature* **578** 66-69 (2020)
- [46] C. Heil, S. di Cataldo, G. B. Bachelet and L. Boeri, Superconductivity in sodalite-like yttrium hydride clathrates *Physical Review B* **99** 220502(R) (2019)
- [47] J. A. Camargo-Martínez, *et al*, The higher superconducting transition temperature T_c and the functional derivative of T_c with $\alpha^2F(\omega)$ for electron–phonon superconductors *J. Phys.: Condens. Matter* **32** 505901 (2020)
- [48] E. F. Talantsev, Classifying superconductivity in compressed H₃S *Modern Physics Letters B* **33**, 1950195 (2019)
- [49] C. J. Gorter and H. Casimir, On supraconductivity I *Physica* **1** 306-320 (1934)
- [51] C. K. Jones, J. K. Hulm and B. S. Chandrasekhar, Upper critical field of solid solution alloys of the transition elements *Rev. Mod. Phys.* **36** 74- (1964)
- [52] L. P. Gor'kov, The critical supercooling field in superconductivity theory, *Sov. Phys. JETP* **10** 593-599 (1960)

- [53] T. Baumgartner, M. Eisterer, H. W. Weber, R. Flueckiger, C. Scheuerlein, L. Bottura, Effects of neutron irradiation on pinning force scaling in state-of-the-art Nb₃Sn wires *Supercond. Sci. Technol.* **27** 015005 (2014)
- [54] D. Sun, *et al.*, High-temperature superconductivity on the verge of a structural instability in lanthanum superhydride *Nature Communications* **12** 6863 (2021)
- [55] E. Helfand and N. R. Werthamer, Temperature and purity dependence of the superconducting critical field, H_{c2} . II. *Phys. Rev.* **147** 288-294 (1966)
- [56] N. R. Werthamer, E. Helfand and P. C. Hohenberg, Temperature and purity dependence of the superconducting critical field, H_{c2} . III. Electron spin and spin-orbit effects *Phys. Rev.* **147**, 295-302 (1966)
- [57] H. Ninomiya, *et al.*, Superconductivity in a scandium borocarbide with a layered crystal structure *Inorg. Chem.* **58** 15629-15636 (2019)
- [58] H. Xie, *et al.*, Superconducting zirconium polyhydrides at moderate pressures *The Journal of Physical Chemistry Letters* **11** 646-651 (2020)
- [59] W. Zhang, *et al.*, A New superconducting 3R-WS₂ phase at high pressure *J. Phys. Chem. Lett.* **12** 3321-3327 (2021)
- [60] M. Scuderi, *et al.*, Nanoscale analysis of superconducting Fe(Se,Te) epitaxial thin films and relationship with pinning properties *Scientific Reports* **11** 20100 (2021)
- [61] KeYuan Ma, *et al.*, Group-9 transition-metal suboxides adopting the filled-Ti₂Ni structure: A class of superconductors exhibiting exceptionally high upper critical fields *Chem. Mater.* **33** 8722–8732 (2021)
- [62] M. Boubeche, *et al.*, Enhanced superconductivity with possible re-appearance of charge density wave states in polycrystalline Cu_{1-x}Ag_xIr₂Te₄ alloys *Journal of Physics and Chemistry of Solids* **163** 110539 (2022)
- [63] E. F. Talantsev, Advanced McMillan's equation and its application for the analysis of highly-compressed superconductors *Superconductor Science and Technology* **33** 094009 (2020)
- [64] E. F. Talantsev, The electron-phonon coupling constant and the Debye temperature in polyhydrides of thorium, hexadeuteride of yttrium, and metallic hydrogen phase III *Journal of Applied Physics* **130** 195901 (2021)
- [65] F. Gross, *et al.*, Anomalous temperature dependence of the magnetic field penetration depth in superconducting UBe₁₃. *Z. Phys. B* **64** 175-188 (1986)
- [66] F. Gross-Alltag, B. S. Chandrasekhar, D. Einzel, P. J. Hirschfeld and K. Andres, London field penetration in heavy fermion superconductors *Z. Phys. B* **82** 243-255 (1991)
- [67] E. F. Talantsev, In-plane p -wave coherence length in iron-based superconductors *Results in Physics* **18** 103339 (2020)
- [68] C. B. Satterthwaite and I. L. Toepke, Superconductivity of hydrides and deuterides of thorium *Phys. Rev. Lett.* **25**, 741-743 (1970)